Induction of Reproducible Brain Infarction by Photochemically Initiated Thrombosis

Brant D. Watson, PhD, W. Dalton Dietrich, PhD,* Raul Busto, BS, Mitchell S. Wachtel, BS, and Myron D. Ginsberg, MD

We have used a photochemical reaction in vivo to induce reproducible thrombosis leading to cerebral infarction in rats. After the intravenous injection of rose bengal, a potent photosensitizing dye, an ischemic lesion was formed by irradiating the left parietal convexity of the exposed skull for 20 minutes with green light (560 nm) from a filtered xenon arc lamp. Animals were allowed to survive from 30 minutes to 15 days after irradiation. Early microscopic alterations within the irradiated zone included the formation of thrombotic plugs and adjacent red blood cell stasis within pial and parenchymal vessels. Scanning electron microscopy revealed frequent platelet aggregates adhering to the vascular endothelium, often resulting in vascular occlusion. Carbon-black brain perfusion demonstrated that occlusion of vascular channels progressed after irradiation and was complete within 4 hours. Histopathological examination at 1, 5, and 15 days revealed that the associated infarct evolved reproducibly through several characteristic stages, including a phase of massive macrophage infiltration. Although cerebral infarction in this model is initiated by thrombosis of small blood vessels, the fact that the main pathological features of stroke are consistently reproduced should permit its use in assessing treatment regimens. Further, the capability of producing infarction in preselected cortical regions may facilitate the study of behavioral, functional, and structural consequences of acute and chronic stroke.

Watson BD, Dietrich WD, Busto R, Wachtel MS, Ginsberg MD: Induction of reproducible brain infarction by photochemically initiated thrombosis. Ann Neurol 17:497–504, 1985

Although thrombosis of the cerebral vasculature accounts for approximately 75% of human stroke cases, currently available animal models tend to be less than satisfactory in their ability to simulate the clinical disorder in a reproducible and physiologically relevant manner. The induction of focal ischemia in rodents [21, 28, 29, 31, 37], cats [22, 27], dogs [42], and subhuman primates [6, 17, 25] by surgical occlusion of major arteries can be criticized in that it circumvents the participation of platelet aggregation as the primary initiator of the ischemic event. Furthermore, the production of ischemia in these models often depends upon an invasive surgical approach, the feasibility of which may be limited by anatomical factors. Infarcts resulting from the intra-arterial injection of microspheres [1, 23] or homologous blood clots [20, 24] may show great fluctuations in size and location.

A different approach to the problem of producing thrombosis in situ is based on photochemically stimulated platelet aggregation, i.e., aggregation facilitated by the interaction of light with an organic dye that has been injected into the circulation. Reproducible focal thrombosis in pial vessels of craniotomized mice [35, 36] or cats [33] has been achieved by irradiating the vessels with blue light after systemic injection of sodium fluorescein dye. We have modified this procedure to develop a minimally invasive reproducible method of inducing cerebral infarction after photochemically initiated thrombosis in rat cortex. This work is based on our observation that another fluorescein dye, rose bengal (disodium tetraiodo-tetrachlorofluorescein), photochemically facilitates in vivo platelet aggregation in brain parenchymal vessels of the rat without the necessity of disturbing the calvarium, which is translucent to the irradiating light.

In the present study, we describe a method of inducing brain infarction photochemically, document the vascular events leading to this infarction, and assess the consistency of the evolving lesion.

Methods

Animal Preparation

Male Wistar rats weighing between 290 and 370 gm were initially anesthetized with halothane and maintained on 1.5% halothane in a mixture of 70% nitrous oxide and 30% oxygen delivered by a closely fitting face mask. The scalp was

From the Cerebral Vascular Disease Research Center and the Departments of Neurology and *Anatomy and Cell Biology, University of Miami School of Medicine, Miami, FL 33101.

Received Jul 25, 1984, and in revised form Oct 15. Accepted for publication Oct 18, 1984.

Address reprint requests to Dr Watson, Department of Neurology (D4-5), University of Miami School of Medicine, P.O. Box 016960, Miami, FL 33101.

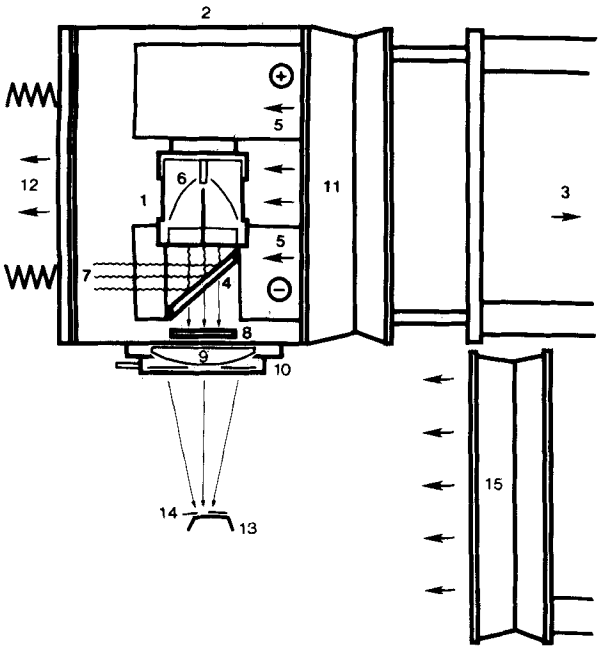

Fig 1. Arc lamp irradiation system. An ILC Technology 300-watt xenon arc lamp (1) *is mounted vertically in its modified housing* (2) *(cutaway view) on an optical rail* (3) *(not shown). The lamp and a Corion hot mirror* (4) *are mounted in a network of heat-dissipating metal vanes* (5), *which also serve as electrodes for the lamp. The lamp contains a parabolic reflector* (6) *attached to a ceramic housing (not shown) that isolates the lamp electrodes. White light, collected and partially collimated by the parabolic reflector, is prefiltered by the hot mirror, which reflects ultraviolet and infrared radiation* (7). *The remaining visible light is spectrally modified by a Corion interference filter* (8) *to produce a band width of 60 nm, centered at 560 nm. The filtered beam is focused by a 75 mm focal length fused silica lens* (9). *The intensity of the irradiation beam is controlled by an optical aperture* (10) *in conjunction with the current control knob on the lamp power supply (not shown). The lamp and optical components are cooled by a fan in its housing* (11) *(airflow designated by* arrows); *this fan also ejects photochemically produced ozone through an exhaust hose* (12). *The rat is mounted with its skull surface* (13) *at the focal point, 6 cm from the face of the optical aperture. A 4 × 6 mm optical aperture* (14) *made from brass shim stock is mounted on the skull and taped in place. An auxiliary fan* (15) *with a 57 L/sec output removes heat from the irradiated tissue zone and maintains tissue temperature at 37.5 to 38.5°C. At the focal point the beam intensity is 0.64 watts/cm^2 as measured by a Laser Precision Corporation pyroelectric detector.*

incised and retracted to expose the skull. From a 7.5 mg/ml saline solution of rose bengal (MW, 1018), which had been subjected to 0.22 μm filtration, an aliquot was injected via a tail vein cannula. By injecting 0.133 ml/100 gm rat weight, a total body dye concentration of 1 mg/100 gm was produced. The calculated blood concentration was 168 μM, based upon an assumed tissue blood volume of 5.7 ml/100 gm [9]. In the somatosensory cortex, which is the region to be irradiated, the tissue blood volume is 0.89 ml/100 gm [9]. With this cerebral blood volume, the dye concentration given above, and a measured molar extinction coefficient at 560 nm of 8.0 × 10^4 M^{-1} cm^{-1}, the dye absorbance per millimeter of tissue is calculated to be 0.012.

The rat's head was positioned at the beam focus of a vertically mounted xenon arc lamp (Fig 1). The beam was spectrally filtered into a band 60 nm wide centered at 560 nm (the absorption maximum of rose bengal). The geometric center of the left parietal calvarium was marked, and a 4 × 6 mm optical aperture made of brass shim stock was mounted onto the skull by strips of white tape. Preliminary irradiations showed that the rat skull was sufficiently translucent to green light to transmit photochemically effective intensities into internal brain regions, thereby rendering craniotomy unnecessary and ensuring the noninvasive character of the method. Approximately 75 rats were used in these preliminary studies to establish optimal irradiation conditions. All animals in the series underwent 20 minutes of irradiation except those studied with the scanning electron microscope.

To prevent heat-mediated tissue damage, which could contribute to tissue injury, the irradiated skull surface was cooled with a high-speed fan with a capacity of 57 L/sec (Fig 1). The fan was turned on 10 seconds before the lamp aperture was opened for it to reach its maximum airflow at the onset of irradiation. In 6 animals, the temperature at several depths within the forming lesion was measured with an implanted thermistor probe to assess the ability of the fan to dissipate heat generated by absorption and scattering of the beam in brain tissue.

Morphological Study

Seven animals were perfused with carbon black to document the sequence of vascular occlusion. Thirty minutes, 4 hours, and 24 hours after 20-minute irradiation, animals were perfused transcardially for 30 seconds with saline solution followed by 50 ml of filtered carbon black (Pelikan AG; Hannover, Germany). Brains were then carefully removed from the cranial vault and placed in fixative consisting of 2.2% paraformaldehyde in a 0.1 M solution of phosphate buffer.

Routine light microscopic analysis was carried out on animals that were allowed to survive for 30 minutes (4 animals), 1 day (5 animals), 5 days (5 animals), and 15 days (3 animals). Rats were anesthetized with halothane and their brains were perfusion-fixed with formaldehyde, glacial acetic acid, and methanol (FAM), 1:1:8 by volume, for 15 minutes after a 30-second saline wash. Brains were left in situ overnight at 4°C before removal from the cranial vault. They were stored in FAM at room temperature until they were blocked, dehydrated, infiltrated, and embedded in paraffin. Paraffin sections (6 μm) of fixed brains were then stained with hematoxylin-eosin for histopathological analysis.

Three animals receiving 5 minutes of irradiation underwent scanning electron microscope analysis. This analysis was carried out to help document mechanisms of vascular occlusion. After irradiation, animals were perfusion-fixed with 0.9% sodium chloride solution followed by 2% paraformaldehyde and 2.5% glutaraldehyde in 0.1 M sodium phosphate buffer. The fixed brain was then removed from the cranial vault and placed in fresh chilled fixative at 4°C for 2 hours. Brains were sectioned into coronal blocks containing the irradiated zone and returned to chilled 0.1 M sodium phosphate buffer at 4°C for 2 hours. Each blocked segment was

mounted on an Oxford Vibratome and completely sectioned at 150 μm in the coronal plane. Methods of tissue processing and scanning electron microscopic analysis have been described previously [10]. Two groups of control animals were allowed to survive for 24 hours after surgical manipulation. To test the effect of irradiation alone, 5 animals were injected with the appropriate aliquot of saline solution not containing rose bengal and were then irradiated for 20 minutes. To determine whether rose bengal could induce observable effects on the nervous tissue in the absence of light, 3 animals were injected with rose bengal but were not irradiated.

Results

Temperature Probe Experiments

With skulls exposed and the beam aperture closed, the average initial cortical temperature at several depths in the zone to be irradiated was found to be 37.3°C in the 6 rats used for this purpose. When the beam aperture was opened, the temperature began to increase immediately and attained its maximum average increase of 1.5°C within 1 minute. The average temperature then decreased as the irradiation proceeded. The average temperature measured at the end of the 20-minute irradiation period was 0.8°C greater than the initial temperature.

Control Animals

The 7 carbon black–perfused animals undergoing 20 minutes of irradiation without rose bengal injection showed no perfusion deficit. The major vascular trunks and smaller arterial branches and venous tributaries of the pial vessels were well demarcated on the surface of the brain. Coronal brain sections taken through the irradiated zone demonstrated large numbers of penetrating vessels coursing throughout the cortex and giving off numerous small branches. Hematoxylin-eosin–stained paraffin sections were unremarkable in both control groups (Fig 2A).

Irradiated Animals

Patchy areas devoid of carbon black were apparent in major trunks of some surface vessels 30 minutes after irradiation. In contrast to controls, smaller branches of the pial vessels were no longer visible. Beneath the irradiated pial membrane a pale cortical region measuring approximately two to three millimeters in diameter was apparent. Coronal sections taken through the irradiated zone demonstrated a decrease in the number of vessels traceable with carbon black in the superficial but not the deeper layers of the cortex. Fairly large vessels (greater than 50 μm) coursing perpendicularly to the pial surface contained regions in which carbon-black filling abruptly stopped and erythrocytes were visible. Other penetrating vessels were completely filled with carbon black, with their branches apparent only in the deeper layers of the irradiated cortex.

A dramatic decrease in the number of irradiated pial vessels traceable with carbon black was observed at 4 hours compared with findings at 30 minutes (Fig 3A). The main branches of the middle cerebral artery, however, were still patent. The pale lesion had increased in surface dimensions to 5 × 7 mm. Coronal sections taken through the infarcted area also demonstrated that the total volume of nonperfused tissue had increased and now extended to the underlying cortical white matter (Fig 3B). The lesion was parabolic in shape and contained a few penetrating vessels coursing through the area. Numerous vessels in the central zone of the lesion were filled with blood, giving the region a reddish appearance. Although petechial hemorrhages were observed occasionally, they were not common. In contrast, the peripheral area of the lesion appeared pale, with few blood-filled vessels. These regions bordered areas containing normally perfused vessels.

A progressive decrease in the number of perfusible vessels was observed on the surface of the cortex 24 hours after irradiation. The irradiated zone appeared white and had not increased in size compared with separate observations made at 4 hours. On coronal sections, the majority of vessels within the irradiated zone exhibited vascular stasis. A few fairly large vessels coursing perpendicularly to the pial surface were still patent, however, and appeared to be the major penetrating branches of the middle cerebral artery.

Light Microscopic Findings

At 30 minutes, pial and parenchymal vessels within the superficial layers of the irradiated cortex frequently showed thrombotic material and red blood cell stasis (Fig 2C, D). No other cellular abnormalities were apparent at this early period.

A poorly staining cortical infarct extending through the entire thickness of the cerebral cortex was apparent after 24 hours in all animals. Neurons appeared angulated and slightly shrunken (Fig 2B). Numerous vacuoles of various sizes were apparent within the neuropil. Parenchymal vessels frequently contained red blood cells and thrombotic material. Some vessels appeared to be collapsed and were surrounded by clear spaces.

A well-demarcated infarct was visible at 5 days, consistently surrounded by a rim of macrophages that had begun to infiltrate the necrotic zone (Fig 4). Parenchymal vessels containing thrombotic material were still apparent coursing through a spongy neuropil that contained unrecognizable neurons. Polymorphonuclear leukocytes were occasionally seen within the neuropil and vessel lumina. Large reactive astrocytes were also observed intermixed with the macrophage layer.

At 15 days, the infarct appeared cystic and contained various sized cavities. Some macrophages were

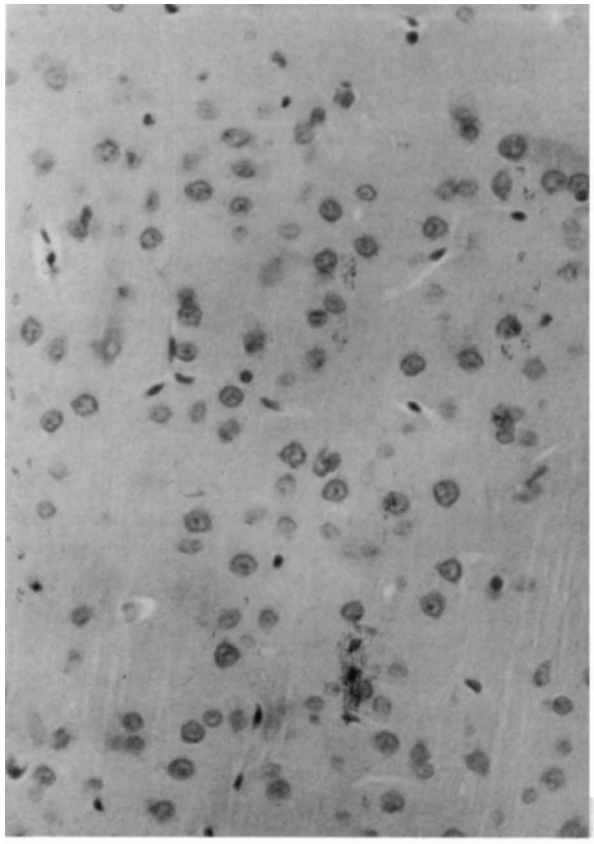

A

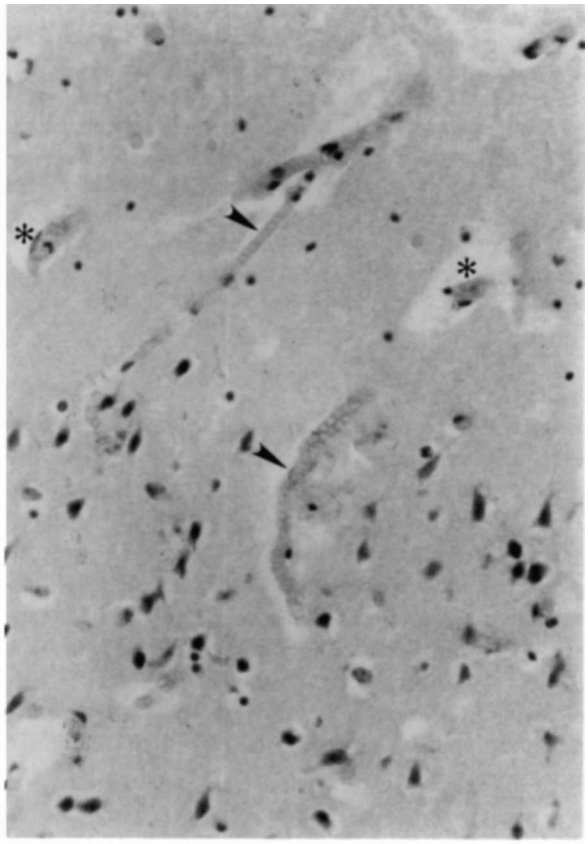

B

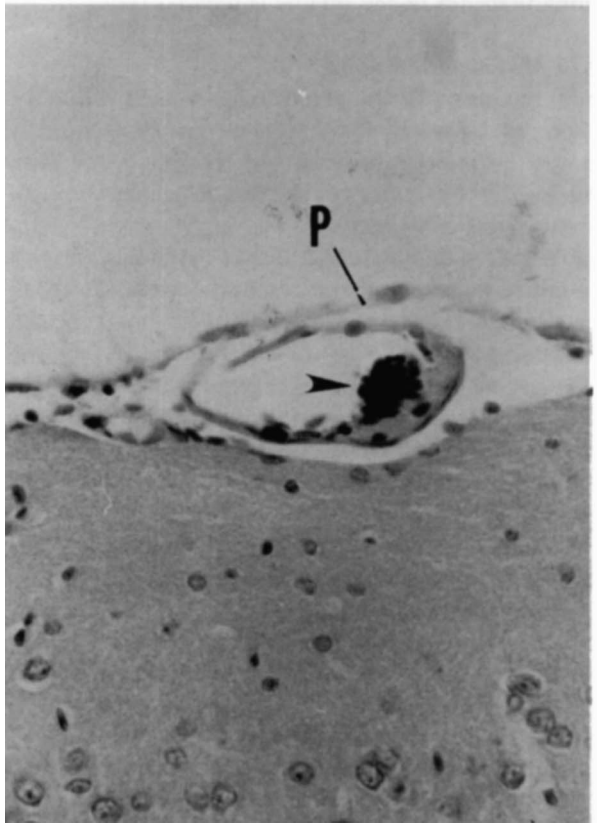

C

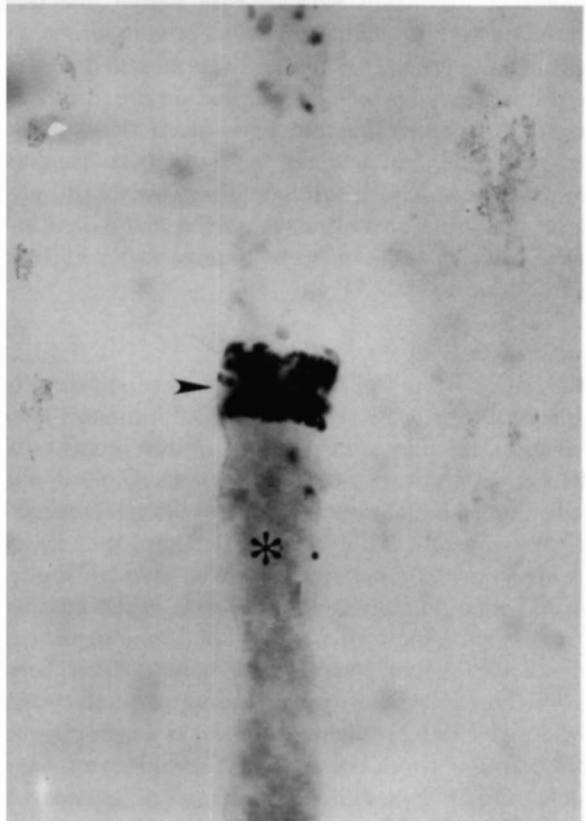

D

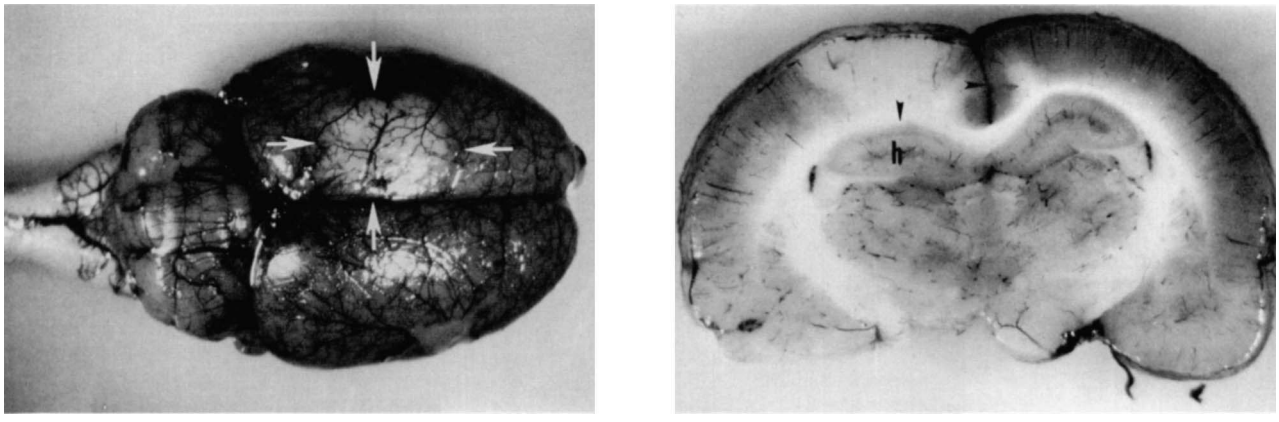

A B

Fig 3. Brain of a rose bengal–injected rat infused with carbon black 4 hours after 20-minute exposure to irradiation with beam centered at 560 nm. (A) The number of patent pial vessels in the irradiated cortex is decreased. (×6 before 50% reduction.) (B) Coronal section bisecting the irradiated zone at the level of the hippocampus (h). *The region of decreased vascular perfusion extends through the entire cortical thickness. Arrowheads indicate sites of structural displacement produced by the developing lesion. (×10 before 50% reduction.)*

still apparent within the central zone of the lesion. Many large astrocytes associated with a newly formed glial scar were also apparent, as were capillaries lying within the necrotic zones.

Ultrastructural Findings

Scanning electron microscopy demonstrated frequent platelet aggregates adhering to luminal surfaces of both large and small parenchymal vessels after only 5 minutes of photoactivation. Platelet aggregation was commonly sufficient to occlude the lumen totally (Fig 5). The aggregated platelets appeared highly irregular in shape with thin, radiating pseudopodia. Endothelial surfaces not obscured by platelets frequently demonstrated focal areas of damage.

Fig 2. Paraffin-embedded sections, stained with hematoxylin-eosin, taken from brains of rats subjected to several different conditions of irradiation and recovery time. (A) Saline-injected sham-operated control animal (×400 before 10% reduction) and (B) rose bengal–injected experimental animal (×375 before 10% reduction) irradiated for 20 minutes and allowed to survive 24 hours. Neuronal and vascular elements appear unremarkable in A but red blood cell stasis (arrowheads) *and perivascular swelling* (star) *are evident in B. The majority of neurons appear shrunken with eosinophilic cytoplasm and pyknotic nuclei. (C and D) Rose bengal–injected animals were subjected to 5 minutes (C) and 20 minutes (D) of irradiation and processed immediately. In C, thrombotic material* (arrowhead) *accumulating within vessels underlying the pial membrane* (P) *is an early indicator of injury (×1,600 before 10% reduction), and in D, development of thrombotic plugs* (arrowhead) *and concomitant red blood cell stasis* (star) *in brain parenchymal vessels are characteristics of vessel injury resulting from prolonged irradiation (×1,800 before 10% reduction).*

Discussion

The present model of photochemically induced thrombotic stroke offers several advantages over previously described methods of producing focal cerebral infarction. Animal preparation is straightforward and does not involve mechanical manipulation of brain blood vessels or parenchyma. Lesion size, severity, and location may be controlled by selecting the appropriate irradiating wavelength and intensity, beam shape and position, duration of light exposure, and dye concentration. The method is virtually noninvasive because of the ability of the translucent skull to transmit the irradiated light. A major advantage of the model is that it does not impede long-term survival. In this series, 15-day survival, when desired, was achieved in all animals.

The mechanism of photoinduced in vivo platelet aggregation in brain vasculature involves geometric as well as biochemical factors. The geometric factors pertain to the transmission of incident light through the intact calvarium. The fraction of light transmitted (T) as a function of depth (x) is given by $T = \exp(-x/\delta)$, where δ, the optical penetration depth, is the depth at which 36.8% [(exp(−1)] of the beam intensity remains. The transmittance of light through human skull has been measured [39]; from these data and a knowledge of the average thickness of the rat's skull in the parietal area (0.5 mm), it can be calculated that the transmitted fraction of 560 nm light presented to the cortical surface of the rat brain is 70%. Similarly, the penetration depth of light through brain tissue has been measured as 0.34 mm at 560 nm in the dog [3], and 0.38 mm at 570 nm in the cat [12]. The injected dye itself accounts for considerably less attenuation of

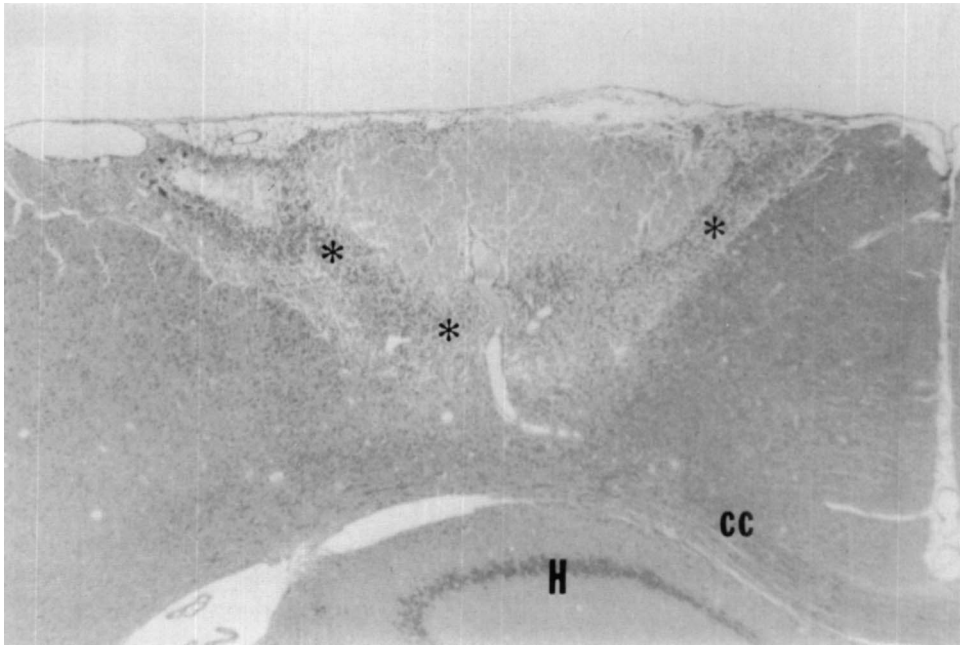

Fig 4. Hematoxylin-eosin–stained section of a chronic brain infarct in an animal injected with rose bengal and irradiated. The infarcted zone is consistent with the region irradiated. At 5 days after irradiation the well-demarcated infarct is surrounded by a rim of macrophages (stars) *infiltrating the necrotic zone.* (cc = *corpus callosum;* H = *hippocampus.*) (×38 *before 25% reduction.*)

the transmitted light. The absorbance calculated per millimeter (see Methods section) translates into an effective penetration depth of 36 mm, so at a depth of 0.34 mm the contribution of the injected dye to attenuation of a 560 nm beam is only 1%.

If one assumes that these optical data, acquired in dog and cat, are representative as well of the rat, one must account for our observation that the thickness of the evolving cortical infarct greatly exceeds the penetration depth of the irradiating light. It is probable that tissue ischemia is initially induced by photochemically stimulated occlusion of the penetrating surface vessels of the neocortex. The pattern of carbon black perfusion observed 30 minutes after the end of irradiation is consistent with this possibility. Subsequently, the evolution of edema in superficial cortical layers may subject the underlying vasculature to compression; this is suggested by the lack of carbon black perfusion observed 4 hours after irradiation.

An explanation is required for the ability of rose bengal to facilitate thrombosis of much larger volumes of brain parenchyma than does sodium fluorescein [33, 35, 36], inasmuch as the penetration depth for green light (absorbed by rose bengal) is comparable to that of blue light (absorbed by fluorescein) [3, 39]. The most likely explanation for the comparative efficacy of rose bengal is that it is the most efficient known photodynamic generator of singlet molecular oxygen, whereas fluorescein is one of the least efficient [14, 32]. For this reason, photochemical effects can be realized in vivo at a much lower blood concentration of rose bengal (170 μM in the present study) than that employed previously for sodium fluorescein (about 7 mM) [33, 36]. The highly electrophilic singlet oxygen originates from active quenching of the lowest excited dye triplet state by molecular oxygen [13]. Peroxidation of susceptible molecules in this manner, termed *dye-sensitized photo-oxygenation,* has been demonstrated with unsaturated fatty acids when the closely related fluorescein dye erythrosin B (disodium tetra-iodofluorescein) is used [8]. The formation of hydroperoxides in unsaturated lipids is facilitated by direct addition reactions of singlet molecular oxygen with isolated double bonds [34]. Erythrosin B and rose bengal have similar abilities to induce photoperoxidative damage to several types of membrane [32, 40]. Impairment of membrane structure and function results from cross-linking reactions, involving free-radical intermediate species, among protein and phospholipid molecules [38].

We suggest that photochemically induced peroxidative reactions may be responsible for producing the endothelial lesions depicted in Figure 5. Similar effects on the endothelium of the aorta [41] and lung [2] have been observed to result from systemic injection of lipid hydroperoxides, and Povlishock and co-workers [33] have proposed a similar mechanism to account for photochemically induced endothelial injury to pial ves-

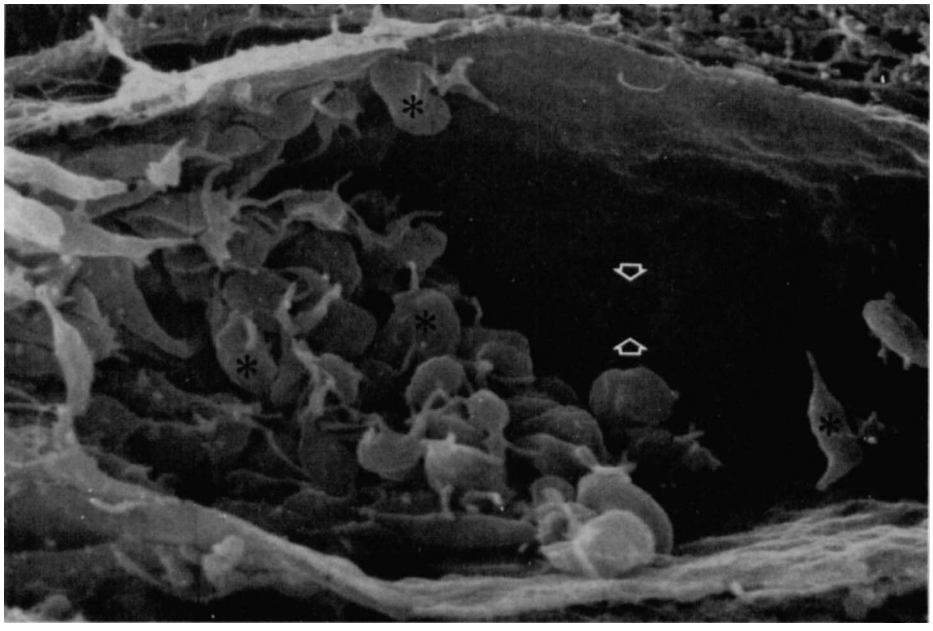

Fig 5. Scanning electron micrograph of a 15-μm cortical vessel taken from a rose bengal–injected animal perfused immediately after a 5-minute irradiation period. Numerous platelets (stars) *adhering to the endothelial surface and to each other result in total occlusion of the vascular lumen. The aggregating platelets demonstrate pseudopodia overlying the endothelium, which appears normal except for occasional small defects* (arrows). *(×7,100 before 25% reduction.)*

sels. Peroxidation of luminal surface lipids may provide the initial stimulus for platelet adhesion and subsequent aggregation. This conjecture is supported by the fact that platelet aggregates are observed only in irradiated tissue zones. In addition, Hermann [19], using fluorescein conjugated to dextran as the photosensitizer, found that quenchers of singlet oxygen inhibited the accumulation of platelets in irradiated arterioles of hamster cheek pouch, and summarized the mechanistic evidence that the activation of platelets was in response to singlet oxygen–mediated induction of endothelial defects.

Besides initiating processes that compromise membrane integrity, photochemically induced peroxidation may inactivate specific endothelial enzymes such as prostacyclin synthetase if, for example, the known inhibitor 15-hydroperoxyarachidonic acid is produced [26]. This process may explain the abnormally intense aggregation of platelets seen in this model [4, 5]. Platelet aggregation appears to proceed physiologically through thrombin stimulation, as indicated by our observations of fibrin deposition in the aggregates [11]. However, the mitigation of the growth rate and volume of the forming thrombus [18], normally induced by prostacyclin in response to thrombin, appears to be largely absent.

In summary, we have demonstrated the feasibility of inducing a cortical infarct of consistent size and location by photochemical methods. Infarct formation appears to be initiated by occlusion of the surface vasculature; extension of the infarct may progress for several hours after cessation of irradiation. By microscopic examination, the developing infarct shows a progression of pathological events similar to those observed in other stroke models [7, 15–17, 30]. Because this method consistently facilitates cortical infarction, the characterization of the early events underlying tissue necrosis may be closely examined. In addition, the model allows for the placement of the ischemic lesion at any portion of the cerebral cortex. This characteristic may facilitate behavioral studies of the consequences of ischemia in specific anatomic–functional regions of brain cortex. Finally, the present model may be suited for the testing of therapeutic agents that specifically influence the platelet response to endothelial damage.

Presented in part at the 108th Annual Meeting of the American Neurological Association, New Orleans, LA, October 2–5, 1983.

Supported by USPHS grant 05820-17 and grant BRSG SO7RR-0563. Dr Dietrich is an Established Investigator of the American Heart Association.

We wish to thank Ofelia Alonso, Mayra Gonzalez-Carvajal, and Isabel Valdes for technical assistance and Helen Valkowitz for typing.

References

1. Allen MB, Dick DAL, Poore BD, Johnson TD: Experimental cerebral infarction. Surg Forum 18:435–436, 1967

2. Anderson WR, Tan WC, Takatori T, Privett OS: Toxic effects of hydroperoxide injections on rat lung. A light microscopical and ultrastructural study. Arch Pathol Lab Med 100:154–162, 1976
3. Bolin FP, Preuss LE, Cain BW: A comparison of spectral transmittance for several mammalian tissues: effects at PRT frequencies. In Doiron DR, Gomer CJ (eds): Porphyrin Localization and Treatment of Tumors. New York, Liss, 1984, pp 211–225
4. Bourgain RH: The inhibition of PGI_2 synthetase within the arterial wall by 15-hydroperoxyarachidonic acid enhances local white platelet thrombus formation. Haemostasis 9:345–351, 1980
5. Bourgain RH, Andries A, Maes L: Effect of cyclooxygenase inhibition on platelet-vessel wall interaction. Haemostasis 13:102–108, 1983
6. Bremer AM, Yamada K, West CR: Experimental regional cerebral ischemia in the middle cerebral artery territory in primates. III. Effects on brain water and electrolytes in the late phase of acute MCA stroke. Stroke 9:387–391, 1978
7. Brierley JB: Pathology of cerebral ischemia. In McDowell FH, Brennan RW (eds): Cerebral Vascular Diseases, Eighth Princeton Conference. New York, Grune & Stratton, 1973, pp 59–66
8. Chan HW-S: Photo-sensitized oxidation of unsaturated fatty acid methyl esters. The identification of different pathways. J Am Oil Chem Soc 54:100–104, 1976
9. Cremer JE, Seville MP: Regional brain blood flow, blood volume, and hematocrit values in the adult rat. J Cereb Blood Flow Metabol 3:254–256, 1983
10. Dietrich WD, Busto R, Ginsberg MD: Cerebral endothelial microvilli: formation following global forebrain ischemia. J Neuropathol Neurol 43:72–83, 1984
11. Dietrich WD, Watson BD, Wachtel M, et al: Ultrastructural analysis of photochemically induced thrombotic stroke in rat brain. Stroke 15:191, 1984
12. Doiron DR, Gomer CJ, Fountain SW, Razum NJ: Light penetration in tissue: its effect on porphyrin detection and quantification by fluorescence *in vivo*. Photochem Photobiol 37 (suppl):S92, 1983
13. Foote CS: Photosensitized oxidation and singlet oxygen: consequences in biological systems. In Pryor WA (ed): Free Radicals in Biology, Vol 2. New York, Academic, 1976, pp 85–134
14. Gandin E, Lion Y, Van de Vorst A: Quantum yield of singlet oxygen production by xanthene derivatives. Photochem Photobiol 37:271–278, 1983
15. Garcia JH: Experimental ischemic stroke: a review. Stroke 15:5–14, 1984
16. Garcia JH, Cox JV, Hodgins WR: Ultrastructure of the microvasculature in experimental cerebral infarction. Acta Neuropathol 18:273–295, 1971
17. Garcia JH, Kamijyo Y: Cerebral infarction: evolution of histological changes after occlusion of a middle cerebral artery in primates. J Neuropathol Exp Neurol 33:408–421, 1974
18. Harlan JM, Harker LA: Hemostasis, thrombosis, and thromboembolic disorders. The role of arachidonic acid metabolites in platelet-vessel wall interactions. Med Clin North Am 65:855–889, 1981
19. Hermann KS: Platelet aggregation in the hamster cheek pouch by a photochemical process with excited fluorescein isothiocyanate-dextran. Microvasc Res 26:238–249, 1983
20. Hill NC, Millikan CH, Wakim KG, Sayre GP: Studies in cerebrovascular disease. VII. Experimental production of cerebral infarction by intracarotid injection of homologous blood clot. Preliminary report. Mayo Clin Proc 30:625–633, 1955
21. Ito U, Spatz M, Walker JT, Klatzo I: Experimental cerebral ischemia in mongolian gerbils. I. Light microscopic observations. Acta Neuropathol (Berl) 32:209–223, 1975
22. Kamijyo Y, Garcia JH, Cooper J: Temporary regional cerebral ischemia in the cat: a model of hemorrhagic and subcortical infarction. J Neuropath Exp Neurol 36:338–350, 1977
23. Kogure K, Busto R, Scheinberg P, Reinmuth OM: Energy metabolites and water content in rat brain during the early stages of development of cerebral infarction. Brain 97:103–114, 1974
24. Kudo M, Aoyama A, Ichimori S, Fukunage N: An animal model of cerebral infarction. Homologous blood clot emboli in rats. Stroke 13:505–508, 1982
25. Little JR, Sundt TM, Kerr FWL: Neuronal alterations in developing cortical infarction: an experimental study in monkeys. J Neurosurg 40:186–198, 1974
26. Moncada S, Vane JR: Unstable metabolites of arachidonic acid and their role in haemostasis and thrombosis. Br Med Bull 34:129–135, 1978
27. O'Brien MD, Jordan MM, Waltz AG: Ischemic cerebral edema and the blood brain barrier: distributions of pertechnetate, albumin, sodium, and antipyrine in brains of cats after occlusion of the middle cerebral artery. Arch Neurol 30:461–465, 1974
28. Petito CK: Platelet thrombi in experimental cerebral infarction. Stroke 10:192–196, 1979
29. Petito CK: Early and late mechanisms of increased vascular permeability following experimental cerebral infarction. J Neuropathol Exp Neurol 38:222–234, 1979
30. Petito CK, Pulsinelli WA, Jacobsen G, Plum F: Edema and vascular permeability in cerebral ischemia: comparison between ischemic neuronal damage and infarction. J Neuropathol Exp Neurol 41:423–436, 1982
31. Plum F, Posner JB, Alvord EC: Edema and necrosis in experimental cerebral infarction. Arch Neurol 9:563–570, 1963
32. Pooler JP, Valenzeno DP: Dye-sensitized photodynamic inactivation of cells. Med Phys 8:614–628, 1981
33. Povlishock JT, Rosenblum WI, Sholley MM, Wei EP: An ultrastructural analysis of endothelial change paralleling platelet aggregation in a light/dye model of microvascular insult. Am J Pathol 110:148–160, 1983
34. Rawls HR, Van Santen PJ: A possible role for singlet oxygen in the initiation of fatty acid autoxidation. J Am Oil Chem Soc 47:121–125, 1970
35. Rosenblum WI, El-Sabban F: Platelet aggregation in the cerebral microcirculation. Effect of aspirin and other agents. Stroke 40:320–328, 1977
36. Rosenblum WI, El-Sabban F: Dimethyl sulfoxide (DMSO) and glycerol, hydroxyl radical scavengers, impair platelet aggregation within and eliminate the accompanying vasodilation of injured mouse pial arterioles. Stroke 13:35–39, 1982
37. Tamura A, Graham DI, McCulloch J, Teasdale GM: Focal cerebral ischemia in the rat. I. Description of technique and early neuropathological consequences following MCA occlusion. J Cereb Blood Flow Metab 1:53–60, 1981
38. Tappel AL: Lipid peroxidation damage to cell components. Fed Proc 32:1870–1874, 1973
39. Wan S, Parrish JA, Anderson RR, Madden M: Transmittance of nonionizing radiation in human tissues. Photochem Photobiol 34:679–681, 1981
40. Watson BD, Haynes DH: Structural and functional degradation of Ca^{2+}:Mg^{2+}-ATPase rich sarcoplasmic reticulum vesicles photosensitized by erythrosin B. Chem Biol Interact 41:313–325, 1982
41. Yagi K, Ohkawa H, Ohishi N, et al: Lesion of aortic intima caused by intravenous administration of linoleic acid hydroperoxide. J Appl Biochem 3:58–65, 1981
42. Yoshimoto T, Sakamoto T, Suzuki J: Experimental cerebral infarction. Part I: Production of thalamic infarction in dogs. Stroke 9:211–214, 1978